

# Journal of Biomedical Optics

SPIEDigitalLibrary.org/jbo

## **Two-photon microscopy of the mouse cochlea *in situ* for cellular diagnosis**

Xin Yang  
Ye Pu  
Chia-Lung Hsieh  
Cheng Ai Ong  
Demetri Psaltis  
Konstantina M. Stankovic



# Two-photon microscopy of the mouse cochlea *in situ* for cellular diagnosis

Xin Yang,<sup>a</sup> Ye Pu,<sup>a</sup> Chia-Lung Hsieh,<sup>a,b</sup> Cheng Ai Ong,<sup>c</sup> Demetri Psaltis,<sup>a</sup> and Konstantina M. Stankovic<sup>c</sup>

<sup>a</sup>École Polytechnique Fédérale de Lausanne, School of Engineering, Optics Laboratory, BM 4.107, Station 17, CH-1015 Lausanne, Switzerland

<sup>b</sup>California Institute of Technology, Department of Electrical Engineering, 1200 East California Boulevard, MC 136-93, Pasadena, California 91125

<sup>c</sup>Harvard Medical School, Department of Otolaryngology and Massachusetts Eye and Ear Infirmary, Department of Otolaryngology, Boston, Massachusetts

**Abstract.** Sensorineural hearing loss is the most common type of hearing loss worldwide, yet the underlying cause is typically unknown because the inner ear cannot be biopsied today without destroying hearing, and intracochlear cells have not been imaged with resolution sufficient to establish diagnosis. Intracochlear imaging has been technologically challenging because of the cochlea's small size and encasement in bone. We report, for the first time, imaging of the mouse cochlea *in situ* without exogenous dyes, through a membranous round window, using a near-infrared femtosecond laser as the excitation and endogenous two-photon excitation fluorescence (TPEF) and second harmonic generation as the contrast mechanisms. We find that TPEF exhibits strong contrast allowing cellular, and even subcellular resolution, and detection of specific, noise-induced pathologic changes. Our results demonstrate that the round window provides a useful access to the cochlea through the middle ear, and they motivate future development of a new and efficient diagnostic tool based on two-photon micro-endoscopy. © The Authors.

Published by SPIE under a Creative Commons Attribution 3.0 Unported License. Distribution or reproduction of this work in whole or in part requires full attribution of the original publication, including its DOI. [DOI: [10.1117/1.JBO.18.3.031104](https://doi.org/10.1117/1.JBO.18.3.031104)]

Keywords: two photon microscopy; cochlea; diagnosis; noise trauma.

Paper 12423SS received Jul. 4, 2012; revised manuscript received Sep. 11, 2012; accepted for publication Sep. 28, 2012; published online Nov. 19, 2012.

## 1 Introduction

Hearing loss is the most common sensory deficit in the world and the most common congenital anomaly.<sup>1</sup> The most frequent type of hearing loss affects delicate mechanosensory and neural structures inside the inner ear and is known as sensorineural hearing loss (SNHL). For the vast majority of people with SNHL, the underlying cause is not known because the inner ear cannot be biopsied today without destroying hearing, and clinically used computed tomography (CT) and magnetic resonance imaging (MRI) scans have insufficient resolution to establish cellular diagnosis. Consequently, therapeutics for SNHL are relatively crude and generalized. Intracochlear imaging has been technologically challenging primarily because of the limited access due to the surrounding bone and because of small and narrow cochlear chambers.

There are two natural openings into the inner ear: the round and oval windows. The round window is covered by a membrane that oscillates with opposite phase to vibrations entering the inner ear through the oval window, which articulates with the bony stapes. Most hearing loss, including noise-induced and age-related hearing loss, starts and is most prominent in the cochlear region close to the round window. Accessing the round window has been of intense interest for vibratory transducer implants,<sup>2</sup> intra-tympanic drug delivery,<sup>3,4</sup> and cochlear implants.<sup>5</sup>

Optical techniques are particularly well-suited for imaging of the delicate intracochlear structures because they offer a significantly higher spatial resolution and lower cost compared with

CT<sup>6</sup> and MRI<sup>7</sup> scans. Recently, optical techniques of confocal fluorescence microscopy<sup>8</sup> and optical coherence tomography<sup>9,10</sup> have been applied to the cochlea. Confocal microscopy is advantageous for its high resolution and deep penetration depth, yet disadvantageous for the necessity of exogenous labeling. The exogenous dyes or antibodies may result in tissue deformation and artifacts, thus limiting interpretation of the results. Two-photon excitation fluorescence (TPEF) microscopy<sup>11</sup> is a nonlinear optical imaging technique with important advantages over conventional confocal microscopy.<sup>12–15</sup> Because of the near-infrared excitation wavelength, TPEF microscopy provides a much deeper penetration, reduced photo-damage, and improved detection sensitivity while maintaining a spatial resolution comparable with confocal microscopy, making it particularly suitable for imaging inside tissues.<sup>16,17</sup> TPEF microscopy has been widely used in biology and medicine, including imaging of brain tissue,<sup>18</sup> lymph nodes,<sup>19</sup> and blood flow.<sup>20</sup> Recently, TPEF microscopy has been used to study the metabolic state of the organ of Corti through the native emission of nicotinamide adenine dinucleotide (NAD) by viewing a small region through a hole drilled in the cochlear bone.<sup>21</sup>

In this paper we show that two-photon microscopy through the round window provides high-quality images of intracochlear cells, including sensory hair cells and cochlear neurons. We use near-infrared femtosecond laser as the excitation and endogenous TPEF and second harmonic generation (SHG) as the contrast mechanisms to image intracochlear cells without any exogenous labeling and without physically opening the cochlea. These images reveal tissue structures at the cellular level resolution with excellent signal-to-noise ratio. Our imaging strategy has important implications for speedy translation to clinics

Address all correspondence to: Konstantina M. Stankovic, Massachusetts Eye and Ear Infirmary, 243 Charles St, Boston MA 02114. Tel: 617.573.3972; Fax: 617.573.3939; E-mail: [konstantina\\_stankovic@meei.harvard.edu](mailto:konstantina_stankovic@meei.harvard.edu)

because the use of exogenous fluorescent dyes is highly constrained, and the use of transgenic fluorescent proteins is not yet allowed in clinics. Moreover, the assessment of damage based on morphology is more robust compared to the measurement of fluorescence intensity or spectral composition. Our results show clear advantages over imaging techniques based on one-photon processes. The quality of the TPEF-based images and the lack of need for staining or decalcification lead to great potential for new and efficient diagnostic tools for hearing loss if a TPEF-based approach is implemented using a fiber-based two-photon microendoscopy.

## 2 Materials and Methods

### 2.1 Animal Groups and Acoustic Overexposure

Male mice of the CBA/CaJ strain were used in this study. Six-week-old mice ( $N = 12$ ) were exposed to an octave band noise of 8 to 16 kHz at 106 dB SPL for 2 h. This noise is known to cause permanent cellular damage, which is maximal close to the round window and decreases from cochlear base to apex. Animals were unrestrained during noise exposure within cells in a subdivided cage (1 animal/cell). The cage was suspended in a small, reverberant chamber, directly below the horn of the sound-delivery loudspeaker, as previously described.<sup>22</sup> Noise calibration to target SPL was performed immediately before each exposure session. Unexposed age- and sex-matched mice served as controls ( $N = 12$ ).

All animal procedures were approved by the Animal Care and Use Committee of the Massachusetts Eye and Ear Infirmary and Ecole Polytechnique Federale de Lausanne.

### 2.2 Cochlear Extraction

The noise-exposed and control mice were sacrificed two weeks after the exposure to allow the wound in the acoustically traumatized organ of Corti to heal so as to bring out permanent, irreversible changes. This mimics the condition that is typically encountered in clinics, where people present with permanently wounded rather than freshly wounded cochleae. The animals were intracardially perfused with 4% paraformaldehyde in 0.1 M phosphate buffer. The left inner ears were extracted

[Fig. 1(a)], stored in 4% paraformaldehyde at room temperature, and imaged within a week of harvest to ensure a strong signal. The right ears were extracted and processed as described in Sec. 2.4.

A separate group of 8-week-old unexposed animals ( $N = 10$ ) was sacrificed, and their cochleae were extracted without using intracardiac or intracochlear fixatives. These unstained cochleae were imaged within 5 min of extraction to determine endogenous TPEF without chemical fixatives.

### 2.3 Two-Photon Microscopy of the Cochlea *In Situ*

The round window was used as the optical access for two-photon imaging of the intracochlear structures *in situ*, without opening or slicing the cochlea. The inner ears were mounted in an elastic mold made of 1% agarose in water and oriented with the round window facing the microscope objective.

The two-photon images were acquired using a Leica SP5 multiphoton microscope system equipped with a mode-locked Ti:Sapphire laser (Coherent Chameleon) as the light source. The excitation wavelength was 812 nm, and the pulse width was 140 fs. The TPEF and SHG signals were collected in a reflective configuration through the same microscope objective (Leica HCX APO 20×1.0 water immersion). After a 680-nm short-pass filter to eliminate the excitation light, the signals were sent to two photomultiplier tubes (PMTs) for simultaneous TPEF and SHG detection through bandpass filters centered at 525 nm (50 nm bandwidth) and 406 nm (10 nm bandwidth), respectively. The average excitation power measured at the focal plane was ~10 mW resulting in a peak intensity of approximately  $7 \times 10^{11}$  W/cm<sup>2</sup>. The pixel dwell time was chosen between 2 and 8  $\mu$ s according to the signal intensity from different types of samples. For all images, intensities were averaged over eight consecutive frames.

The TPEF images were compared with the images obtained using Zeiss LSM 700 under both one-photon excitation fluorescence (OPEF) confocal microscope and wide-field transmission microscope modes. In the OPEF confocal microscopy, the excitation wavelength was 405 nm, and the emission wavelength was 500 to 550 nm. In both imaging modes, the objective used was a Zeiss N-achromat 20×0.5 NA water immersion objective.

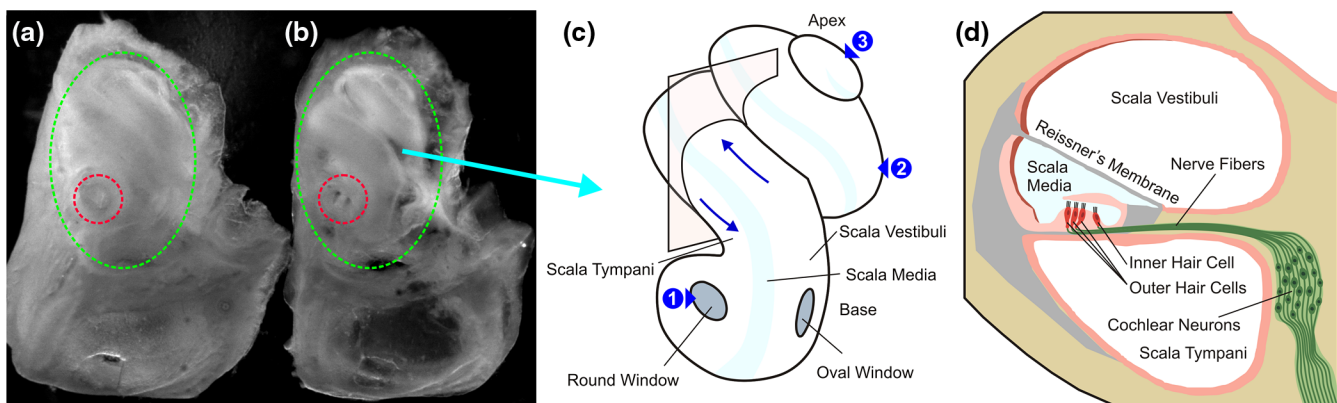


**Fig. 1** Mouse cochlea as seen in dark-field microscopy before (a) and after (b) decalcification. (Details about decalcification are stated in the appendix.) The helical structure of the cochlea is clearly visible in the decalcified sample. The red dashed line encircles the round window, and the green dashed line encircles the cochlea, which is schematized in (c). The blue arrows in (c) indicate the travelling direction of the acoustic waves. The numbers in blue circles mark the imaging locations used in experiments described in Figs. 3 to 8. A cross-sectional diagram cut at the light pink plane is schematized in (d) to illustrate the inner structure of the cochlea. Cochlear bone is shown in beige. The sensory hair cells are located within the organ of Corti.

## 2.4 Histologic Preparation of Cochlear Sections

The right inner ears were removed, postfixed, decalcified in 0.1 M EDTA, dehydrated, embedded in paraffin, serially cut ( $10\ \mu\text{m}$  thickness) and mounted on microscope slides. Select ears were stained with 1% osmium tetroxide prior to decalcification, embedded in Araldite and serially sectioned ( $20\ \mu\text{m}$  thickness), as previously described.<sup>23</sup>

## 3 Results and Discussions

To evaluate the effectiveness of TPEF as an intrinsic contrast for the imaging of the organ of Corti, we first imaged a paraffin-embedded histologic section using TPEF and compared it to the wide-field transmission microscopy image of a similarly oriented, osmium-stained section (Fig. 2). The main structures of interest, namely the inner and outer hair cells (marked in red and green dashed circles, respectively), are clearly revealed in the TPEF image.

Using the round window as the optical access, we next obtained TPEF images of the intracochlear structures *in situ*, without decalcifying or sectioning the cochlea, as shown in Fig. 3(a). We compared them with the images obtained using OPEF and wide-field transmission microscopy with the same magnification, as displayed in Fig. 3(b) and 3(c), respectively.

The resolution of the TPEF and OPEF images is  $\sim 350\ \text{nm}$ , while the resolution of the wide-field transmission microscopy is  $\sim 375\ \text{nm}$ . This is roughly equal to the images we can expect to obtain using microendoscopy-based imaging with the same NA from the middle ear space. Rows of hair cells are seen with sharp details and high signal-to-noise ratio (SNR) when TPEF is used [Fig. 3(a)]. The OPEF image demonstrates fewer details and a lower SNR [Fig. 3(b)], due to linear

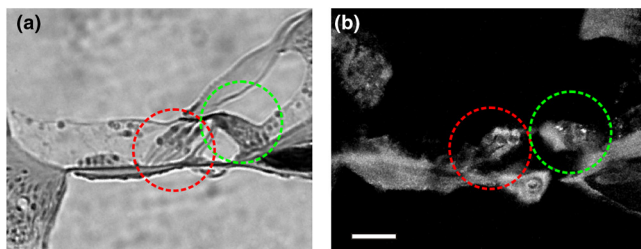


**Fig. 2** (a) Wide-field transmission microscopy of an osmium-stained section of the organ of Corti; (b) TPEF image of a similarly positioned unstained section. In both panels, the red dashed line encircles the three outer-hair cells, and the green dashed line encircles the inner hair cell. The scale bar is  $10\ \mu\text{m}$  (a) (b). The pixel size is  $375\ \text{nm}$  (a) or  $170\ \text{nm}$  (b).

dependence of excitation/emission, instead of the square dependence in TPEF. The wide-field transmission image is blurry [Fig. 3(c)], mainly due to the lack of axial resolution (optical sectioning) and strong scattering from the surrounding bone. The image contrast, defined as the ratio of the mean intensity of the hair cell region to the mean intensity of the imaging plane  $10\ \mu\text{m}$  above the hair cell, are  $\sim 4$  and  $\sim 2$  for TPEF and OPEF images, respectively. The SNR, defined as the ratio of the mean intensity of the hair cell region to the standard deviation of the background in the peripheral area of the same imaging plane, is  $\sim 20$  and  $\sim 10$  for TPEF and OPEF images, respectively. The organ of Corti region is about  $500\ \mu\text{m}$  below the plane of the round window. The round window opening has a diameter of  $\sim 700\ \mu\text{m}$ . The resulting viewing angle onto the organ of Corti through the round window is  $\sim \pm 44\ \text{deg}$ . The collection angles of the objectives used for TPEF and OPEF are  $\sim \pm 49\ \text{deg}$  and  $\sim \pm 25\ \text{deg}$ , respectively. The TPEF objective used is better than the OPEF objective in the efficiency of signal collection. This might also contribute to the dimmer signal in the OPEF images. However, since the signal levels in all three cases are much stronger than the detector noises, we believe that the optical sectioning capability of TPEF is the major contributor to the enhanced image quality compared to OPEF.

The images shown in Fig. 3 were obtained from fixed cochlear samples. An advantage of fixed samples is that tissue degradation is halted so that imaging approaches can be developed and optimized *ex vivo* before eventual studies *in vivo*. Although the paraformaldehyde fixative that we used is known to be superior to other fixatives in preserving cell fluorescence while limiting background fluorescence,<sup>24</sup> the fixative can nonetheless be fluorescent. To determine if the recorded TPEF was indeed endogenous and not accidental due to the fixative, we imaged freshly harvested, unfixed cochleae. A representative result obtained within 5 min of cochlear extraction is shown in Fig. 4. The image shows the same hair cell structures as observed in the fixed samples shown in Fig. 3 from a different viewing angle. The intensity of the fluorescence is brighter in the freshly harvested, unfixed samples than in the fixed samples. Encouraged by the finding that the observed TPEF signal in the fixed samples is primarily due to endogenous TPEF, we pursued further studies in the fixed samples.

Figure 5 shows the TPEF images of the organ of Corti obtained through the round window of an intact cochlea. To better visualize the overall three-dimensional (3-D) structure, we recorded a stack of images in a volume and render them using maximum intensity projection (MIP) when necessary.

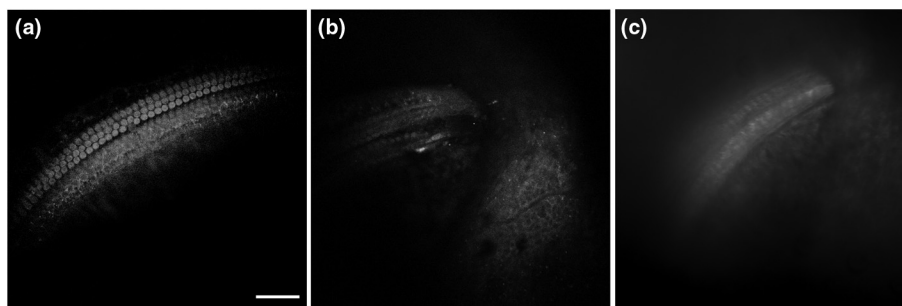


**Fig. 3** Images of the organ of Corti through the round window taken at location 1 schematized in Fig. 1(c) using (a) TPEF microscopy, (b) OPEF microscopy, and (c) wide-field transmission microscopy with the same magnification. TPEF microscopy shows better visual acuity and signal-to-noise ratio compared to the other methods. Scale bar:  $50\ \mu\text{m}$ . Pixel size:  $170\ \text{nm}$  (a) (b) or  $375\ \text{nm}$  (c).

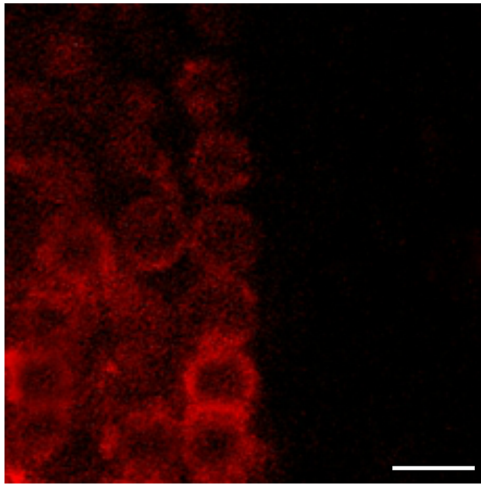


**Fig. 4** A TPEF image of the organ of Corti viewed through the intact round window of an unfixated, unstained cochlea *in situ*. The image was taken within 5 min of cochlear harvest. Rows of hair cells are clearly seen, similar to those observed in Fig. 3(a). The scale bar is 10  $\mu\text{m}$ . The pixel size is 170 nm.

This simple approach revealed a clear distinction between healthy and noise-damaged organ of Corti. The images were obtained at location 1 schematized in Fig. 1(c). Figure 5(a) shows an MIP of the 3-D image stack of the entire hook region. Figure 5(b) through 5(d) shows images of three selected planes with 10  $\mu\text{m}$  distance from each other. TPEF from most cellular tissues exhibits strong contrast, based on which hair cells and supporting cells are clearly identifiable. Due to its weak intrinsic fluorescence, the stereocilia on the apical surface of the hair cell are not visible in the images. The appearance and quality of the TPEF images is similar to the images of cochlear whole-mounts. Despite the resemblance, we emphasize that our images were

acquired from intact cochleae through the round window. Indeed, an important strength of our approach is that high resolution images of the organ of Corti can be obtained through the round window of an intact cochlea without the invasiveness and terminal nature of whole-mount preparations. The SHG channel is likely from the myelin sheath surrounding neuronal axons between neuronal somata.<sup>25</sup> Noise-exposed cochleae were imaged in the same orientation for comparison. Figure 5(e) is a maximum intensity projection (MIP) of the 3-D image stack of the entire hook region. Figure 5(f) through 5(h) shows images of three selected planes with 10  $\mu\text{m}$  distance. Substantial damage and loss of hair cells were evident after noise exposure. Outer hair cells, which are known to be most sensitive to noise trauma, were missing altogether [Fig. 5(g) and 5(h)] while inner hair cells were decimated [Fig. 5(g) and 5(h)]. The SNR for all these images are  $\sim 20$ . Assessment of cochlear regions away from the round window is provided in appendix, including Figs. 6 and 7.

TPEF microscopy was also capable of imaging cochlear neurons at the cellular level through the encasing cochlear bone instead of through the round window (Fig. 8). The TPEF channel (red) reveals the neural somata, the average size of which is  $\sim 25 \mu\text{m}$ , approximately three to four times bigger than the hair cells. This leads to an opportunity to diagnose hearing problems of neural origin.

Our finding of substantial TPEF in cochlear hair cells is consistent with the previous reports.<sup>21,26-28</sup> A major endogenous fluorophore in the inner ear is flavin adenine dinucleotide,<sup>28,29</sup> whose peak of emission ( $\sim 520 \text{ nm}$ ) coincides with the TPEF signal that we recorded. Our results, combined with the fact that the sensory epithelium of the inner ear has one of the highest tissue concentrations of flavin adenine dinucleotide known, strongly motivate future development of TPEF-based microendoscopy for cellular diagnosis of sensorineural hearing loss.

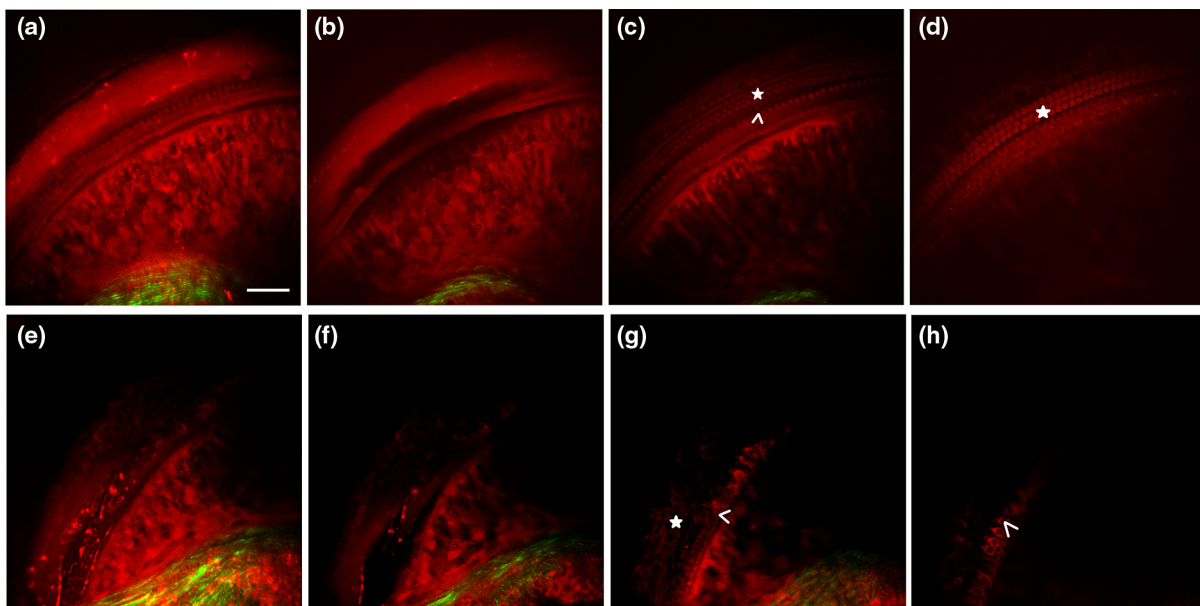


**Fig. 5** Images of the organ of Corti seen through the round window [location 1 in Fig. 1(c)] of unexposed (a–d) and noise-exposed (e) through (h) cochleae. A maximum intensity projection (MIP) of a  $x$ - $y$ - $z$  3D scan of the entire hook region (a) and (e) and  $x$ - $y$  scanning images of three different planes with 10  $\mu\text{m}$  distance (b) through (d) and (f) through (h) are shown. In all panels, the red channel is TPEF, and the green channel is endogenous SHG. The scale bar is 50  $\mu\text{m}$  and the pixel size is 170 nm. The asterisk points to the three rows of outer hair cells (c) and (d), which are missing in the noise-exposed cochleae (g). The arrowhead points to the row of inner hair cells (c), which are decimated after noise exposure (g) and (h).

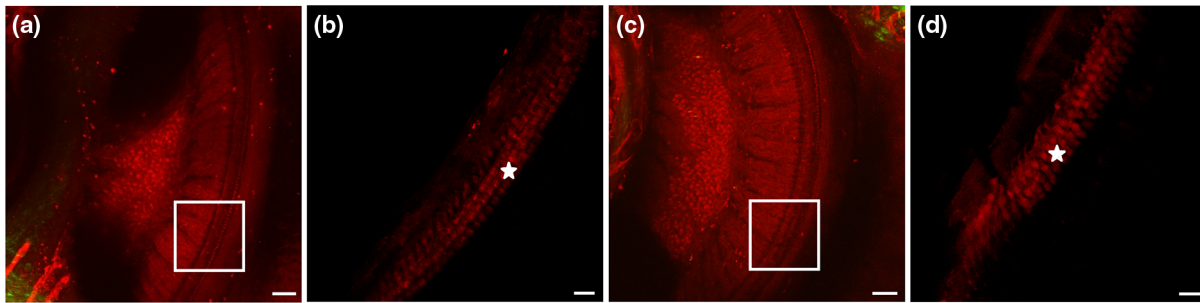


**Fig. 6** Images of the upper basal turn of the organ of Corti from a decalcified mouse cochlea [location 2 in Fig. 1(c)]. MIP of 3-D x-y-z scanning images from a normal (a) and a noise-exposed (c) cochlea. The zoomed in areas outlined by squares in (a) and (c) are shown in (b) and (d), respectively. The scale bar is 50  $\mu\text{m}$  for (a) and (c), and 10  $\mu\text{m}$  for (b) and (d). The pixel size is 350 nm (a) and (c) or 170 nm (b) and (d). The asterisk points to the three rows of outer hair cells, which are neatly arranged in the unexposed cochleae (b) and disarrayed in the noise-traumatized cochleae (d).

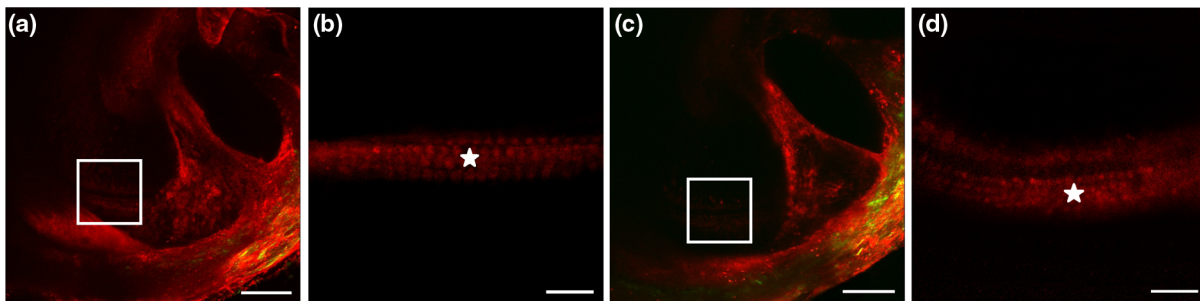


**Fig. 7** Images of the apical turn of the organ of Corti from a decalcified mouse cochlea [location 3 in Fig. 1(c)]. MIP of 3-D x-y-z scanning images from a normal (a) and a noise-exposed (c) cochlea. The zoomed in areas outlined by squares in (a) and (c) are shown in (b) and (d), respectively. The scale bar is 50  $\mu\text{m}$  for (a) and (c), and 10  $\mu\text{m}$  for (b) and (d). The pixel size is 350 nm (a) and (c) or 170 nm (b) and (d). The asterisk points to the three rows of outer hair cells.

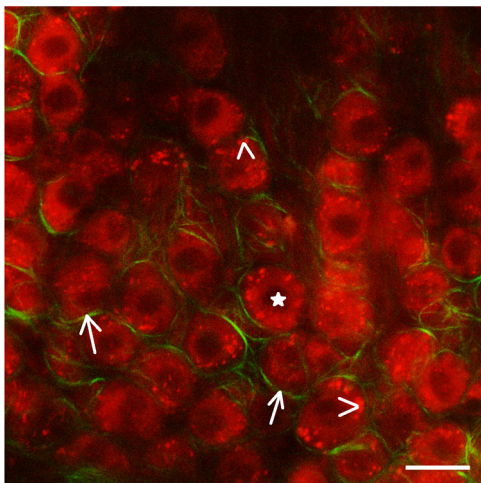


**Fig. 8** A TPEF image of cochlear neurons under intact bone. The red channel is TPEF, which reveals the neural somata. The green channel is endogenous SHG, which possibly originates from the myelinated nerve fibers (white arrows). Intracellular organelles (white arrow heads) and cell nuclei (asterisk) can be seen in neurons. The scale bar is 25  $\mu\text{m}$ . The pixel size is 170 nm.

#### 4 Conclusion

We have investigated TPEF imaging through the round window of the mouse cochlea as a potential diagnostic tool for sensorineural hearing loss. The use of TPEF eliminates the need for exogenous labeling and provides the maximum noninvasiveness in the process. We find that the TPEF yields clear advantages

over OPEF and wide-field transmission microscopy. Our experiments reveal fine cellular structure of the hair cells and allow morphological distinction between healthy and damaged organs of Corti. Furthermore, cochlear neurons have been imaged through the intact bone. Combined, these capabilities provide a working foundation for microendoscopy-based clinical diagnostics of sensorineural hearing loss.

#### Appendix

Imaging through the round window limits diagnostics to the hook region of the organ of Corti, which is the most probable place for the initiation of the sensorineural damage. Decalcification made the cochlear bone transparent, allowing visualization of the basal and apical cochlear turns through the cochlear bone. To assess noise-induced damage along the length of the cochlea, the cochlear bone was decalcified in 80% formic acid and 20% trisodium citrate for 3 h. After decalcification, the penetration depth improved from  $\sim 100 \mu\text{m}$  to  $\sim 2 \text{ mm}$  (limited by the working distance of the microscope objective).

The surface view of the upper basal turn was achieved from the brain side of the cochlea [location 2 marked in Fig. 1(c)]. Figure 6(a) and 6(c) shows the MIP of the image stack at the upper basal turns for normal and noise exposed cochleae, respectively. The cellular level details of the organ of Corti are clearly discernible in the zoomed-in view [Fig. 6(b) and 6(d)]. Noise exposure leads to less cellular damage in the upper basal turn compared with the hook region, as expected based on the noise parameters we used. Although the outer hair cells are

disarrayed after noise trauma [Fig. 6(d)], only a small portion of them are torn off from the basilar membrane in the upper basal turn. The apical turn of the decalcified cochlea demonstrates no noise-induced loss of hair cells (Fig. 7), consistent with the noise parameters we used. The sample was oriented with the apex of the cochlea perpendicular to the microscope objective [location 3 as marked in Fig. 1(c)] in order to achieve a surface view (Fig. 7).

### Acknowledgments

We are grateful for the support of the Bertarelli Foundation.

### References

1. B. Traynor, *The Incidence of Hearing Loss Around the World* (2011).
2. V. Colletti et al., "Treatment of mixed hearing losses via implantation of a vibratory transducer on the round window," *Int. J. Audiol.* **45**(10), 600–608 (2006).
3. A. N. Salt and Y. L. Ma, "Quantification of solute entry into cochlear perilymph through the round window membrane," *Hear. Res.* **154**(1–2), 88–97 (2001).
4. E. E. Swan et al., "Inner ear drug delivery for auditory applications," *Adv. Drug Deliv. Rev.* **60**(15), 1583–1599 (2008).
5. B. Mangus et al., "Surgical techniques in cochlear implants," *Otolaryng. Clin. N. Am.* **45**(1), 69–80 (2012).
6. H. R. Harnsberger et al., "Cochlear implant candidates—assessment with Ct and Mr imaging," *Radiology* **164**(1), 53–57 (1987).
7. J. W. Casselman et al., "Aplasia and hypoplasia of the vestibulocochlear nerve: diagnosis with MR imaging," *Radiology* **202**(3), 773–781 (1997).
8. G. H. MacDonald and E. W. Rubel, "Three-dimensional imaging of the intact mouse cochlea by fluorescent laser scanning confocal microscopy," *Hear. Res.* **243**(1–2), 1–10 (2008).
9. F. Y. Chen et al., "In vivo imaging and low-coherence interferometry of organ of Corti vibration," *J. Biomed. Opt.* **12**(2), 021006 (2007).
10. B. J. F. Wong et al., "Optical coherence tomography of the rat cochlea," *J. Biomed. Opt.* **5**(4), 367–370 (2000).
11. W. Denk, J. H. Strickler, and W. W. Webb, "2-Photon laser scanning fluorescence microscopy," *Science* **248**(4951), 73–76 (1990).
12. A. Monfared et al., "In vivo imaging of mammalian cochlear blood flow using fluorescence microendoscopy," *Otolaryng. Neurotol.* **27**(2), 144–152 (2006).
13. P. T. C. So et al., "Two-photon excitation fluorescence microscopy," *Annu. Rev. Biomed. Eng.* **2**, 399–429 (2000).
14. B. G. Wang, K. Konig, and K. J. Halhuber, "Two-photon microscopy of deep intravital tissues and its merits in clinical research," *J. Microsc. Oxford* **238**(1), 1–20 (2010).
15. W. R. Zipfel, R. M. Williams, and W. W. Webb, "Nonlinear magic: multiphoton microscopy in the biosciences," *Nat. Biotechnol.* **21**(11), 1368–1376 (2003).
16. M. D. Cahalan et al., "Two-photon tissue imaging: seeing the immune system in a fresh light," *Nat. Rev. Immunol.* **2**(11), 872–880 (2002).
17. F. Helmchen and W. Denk, "Deep tissue two-photon microscopy," *Nat. Methods* **2**(12), 932–940 (2005).
18. Z. F. Mainen et al., "Two-photon imaging in living brain slices," *Meth.—Companion Methods Enzymol.* **18**(2), 231–239 (1999).
19. M. J. Miller et al., "Two-photon imaging of lymphocyte motility and antigen response in intact lymph node," *Science* **296**(5574), 1869–1873 (2002).
20. E. Chaigneau et al., "Two-photon imaging of capillary blood flow in olfactory bulb glomeruli," *Proc. Natl. Acad. Sci. U.S.A.* **100**(22), 13081–13086 (2003).
21. L. Tiede et al., "Metabolic imaging of the organ of corti—a window on cochlea bioenergetics," *Brain Res.* **1277**, 37–41 (2009).
22. S. G. Kujawa and M. C. Liberman, "Adding insult to injury: cochlear nerve degeneration after 'temporary' noise-induced hearing loss," *J. Neurosci.* **29**(45), 14077–14085 (2009).
23. K. Stankovic et al., "Survival of adult spiral ganglion neurons requires erbB receptor signaling in the inner ear," *J. Neurosci.* **24**(40), 8651–8661 (2004).
24. C. A. West et al., "Aldehyde fixation of thiol-reactive fluorescent cytoplasmic probes for tracking cell migration," *J. Histochem. Cytochem.* **49**(4), 511–517 (2001).
25. Y. Fu et al., "Second harmonic and sum frequency generation imaging of fibrous astroglial filaments in *ex vivo* spinal tissues," *Biophys. J.* **92**(9), 3251–3259 (2007).
26. E. R. Lewis et al., "Inner-ear—dye injection reveals peripheral origins of specific sensitivities," *Science* **215**(4540), 1641–1643 (1982).
27. S. Sento and T. Furukawa, "Intraaxonal labeling of saccular afferents in the goldfish, *carassius-auratus*—correlations between morphological and physiological-characteristics," *J. Comp. Neurol.* **258**(3), 352–367 (1987).
28. W. F. Sewell and E. A. Mroz, "Flavin adenine-dinucleotide is a major endogenous fluorophore in the inner-ear," *Hear. Res.* **70**(2), 131–138 (1993).
29. W. Zheng et al., "Optimal excitation-emission wavelengths for autofluorescence diagnosis of bladder tumors," *Int. J. Cancer* **104**(4), 477–481 (2003).